INDICIAL AERODYNAMIC MODEL FOR FLUTTER ASSESSMENT IN AXIAL FLIGHT CONSIDERING BLADE AIRFOIL, ROTOR INFLOW AND WAKE PERIODICITY

Jürgen Arnold, DLR German Aerospace Center, Institute of Aeroelasticity, Göttingen, Germany

Abstract

The complete physics of the complex flow field around a rotor is obtained by the application of high-fidelity methods and hence, this is the preferred approach to find the optimal design for aerodynamic and acoustic performance. In comparison, the approach based on indicial aerodynamics ranks as low-fidelity, but offers an efficient and robust method allowing an easy model setup with fast access to basic aeroelastic phenomena at an early design stage. To include both methods in the rotor assessment, an aerodynamic multi-fidelity approach around the same dynamic rotor model is the objective. Hereby, used numerical methods for the low-fidelity approach comprise multibody dynamics together with an unsteady aerodynamic model based on Wagner's function and related enhancements for the general motion of an airfoil section considering heave and pitch motion as well as dynamic rotor inflow and wake periodicity. Since the aerodynamic model is state based, numerical solutions are available from time domain and linearization. The results from linearization allow the assessment of frequency placement and damping of the isolated rotor system.

1. INTRODUCTION

The multibody system SIMPACK (Ref. 1) is used for the setup and simulation of the dynamic rotor model with its flexible blades. Flexibility of the non-rotating blade is described in the multibody system SIMPACK with a modal approach for available finite element models. For the assessment of the rotor in axial inflow condition, an unsteady theory using indicial aerodynamics based on the extended Wagner function in combination with steady two-dimensional airfoil data is applied to the multibody model. This approach allows an efficient and robust flutter assessment of DLR rotor setups in the design process and before entry into service comprising hover and steady axial flight (Ref. 2). According to Table 1, it provides the low-fidelity solution within the choice of three aerodynamic methods for the MBS rotor analysis which form a multi-fidelity aerodynamic approach around a high-fidelity dynamic model as common basis. Hence, the rotor simulation can be adjusted to the required accuracy with a factor of between 50 to 100 in computational time from one fidelity level to the other. Since the approximated Wagner function and the extensions for axial flow are available in a state space model, the evaluation is possible in the time domain or by linearization. Here, linearized results are available in terms of frequency and damping behavior allowing for an initial frequency placement and stability check of the isolated rotor.

Table 1: Multi-fidelity unsteady aerodynamics for coupled rotor simulations with MBS SIMPACK.

Fidelity Level	Coupling	Aerodynamics	Duration	Discretization
Low	UFEL-MBS	Wagner++	Sec-Min / Rev	Blade strip
Mid	UPM-MBS	UPM	Min-Hrs / Rev	Surface panel
High	CFD-MBS	TAU	Days / Rev	Volume

According to Leishman (Ref. 3), unsteady aerodynamic effects of a two-dimensional airfoil result in a lag in the build-up of lift in response to a change in angle-of-attack. In the case of a rotor blade section, a lag in the build-up of thrust and inflow in response to a change in collective pitch is present. With respect to the consideration of relevant rotor wake effects, Leishman (Ref. 3, page 645) concludes: "Dynamic inflow represents another formulation of the problem, where the effects of the wake can be included in a form of differential equations to represent the relationship between the time-dependent inflow velocities and rotor forces and pitching moments. This latter approach is attractive for some problems in rotor analysis, particularly those in flight dynamics and aeroelasticity." As a consequence, the unsteady aerodynamic model considers circulatory contributions from blade airfoil, rotor inflow and wake periodicity to present a rotor blade section. Related indicial response functions for these contributions are implemented as dynamic states in the force model and thus, lead to a tight coupling to the dynamic rotor model on equation level.

2. INDICIAL AERODYNAMIC MODEL

2.1. Model Setup

Assumptions of the implemented aerodynamic model based on 2D thin airfoil theory comprise a bound vortex at ¼ chord together with an evaluation of the downwash at ¾ chord due to basic kinematical constraints as well as the satisfaction of the Kutta flow condition at the trailing edge. The superposition of the overall aerodynamic loads is based on linear contributions and has to consider all steady and unsteady components related to vorticity as well as apparent mass from general motion. They comprise steady values for lift L_0 and moment M_0, inflow-induced lift L_λ related to rotor thrust, motion-induced lift L_1 related to Wagner's function, motion-induced lift L_2 and L_3 related to apparent mass and last not least, the motion-induced moment M_a related to apparent mass moment of inertia. A summary of the components together with their source and application along chord c is given in Table 2.

The Pistolesi concept considering the measurement of downwash at 75% chord holds for all steady and unsteady load components which are related to bound vorticity Γ at quarter chord. All load components related to apparent mass are evaluated for other chord positions or w.r.t. the structural elastic axis. Relevant derivatives of pitch and heave motion need to be strictly measured at the elastic axis (Ref. 4). The available relations are depicted in Figure 1 for the unsteady components.

Table 2: Steady and unsteady aerodynamic load components related to vorticity and apparent mass.

Component	Motion Variable	Source	Application	Remarks
L_0 Steady lift	α	vorticity	bound vortex at ¼ chord	downwash measured at ¾ chord
M_0 Steady moment	α	vorticity	moment reference at ¼ chord	-
L_λ Inflow-induced lift (rotor thrust)	$d\alpha(t)$	vorticity	bound vortex at ¼ chord	downwash measured at ¾ chord
L_1 Motion-induced lift (impulsive motion)	$d\alpha(t)$	vorticity	bound vortex at ¼ chord	downwash measured at ¾ chord
L_2 Motion-induced lift (pitch+heave)	$\ddot{\alpha}(t), \ddot{h}(t)$	apparent mass	centre of pressure at ½ chord	motion measured at elastic axis
L_3 Motion-induced lift (pitch)	$\dot{\alpha}(t)$	apparent mass	centre of pressure at ¾ chord	motion measured at elastic axis
M_a Motion-induced moment (pitch)	$\ddot{\alpha}(t)$	apparent mass moment of inertia	moment reference at elastic axis	motion measured at elastic axis

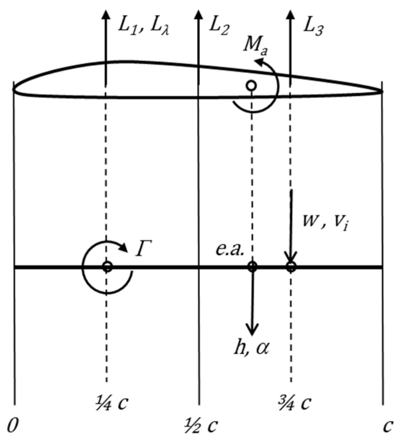

Figure 1: Unsteady aerodynamic load components and chordwise application.

The unsteady aerodynamic model for rotor blade sections takes advantage of indicial response functions $\Phi(t)$ (Ref. 3) which capture the transient changes in aerodynamic variables within the Duhamel superposition integral. These functions model the unsteady aerodynamic response in time domain for variations in angle-of-attack and/or axial inflow. All indicial response functions affect the circulatory part of unsteady lift, are implemented in terms of a state space model in the SIMPACK force element and extended for rotors under axial flow condition. Related contributions include blade airfoil from the Wagner function (Ref. 5), axial dynamic inflow from a non-linear differential equation (Ref. 3) derived out of the results gained by Carpenter and Fridovich (Ref. 6), and wake periodicity as modelled in Loewy's function (Ref. 7) by a complex factor.

2.2. Unsteady Aerodynamics from Motion

The model is based on Wagner's function (Ref. 3) in combination with steady two-dimensional airfoil data and applied to the multibody model. This function considers a two-dimensional thin airfoil of chord length $2b$ in an impulsive motion from rest to uniform velocity U and is commonly used as a model for the circulatory lift development related to a change in angle-of-attack with fixed wing problems. This motion is depicted in Figure 2 for distance τ traveled in semichords during time t. According to Y.C. Fung (Ref. 4), the description of motion induced unsteady lift is extended from an impulsive to general motion including both, pitch and heave motion by taking unsteady apparent mass terms for non-circulatory effects into account.

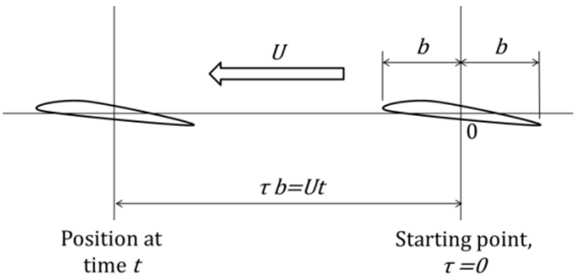

Figure 2: Impulsive motion of an airfoil.

The lift due to circulation acting on the strip of unit span (Ref. 4) follows for an incompressible fluid of density ρ and the downwash w as

(1) $$L_1 = 2\pi b\rho U w \Phi(\tau)$$

where $\Phi(\tau)$ is the Wagner function describing the unsteady lift development towards the steady-state value for increasing distance τ traveled in semichords b. The fast aerodynamic model is based on radial independent strips and has been implemented using the approximation of R.T. Jones (Ref. 8-9) for Wagner's function $\Phi(\tau)$ with

(2) $$\Phi(\tau) = 1 - 0.165e^{-0.0455\cdot\tau} - 0.335e^{-0.300\cdot\tau}$$

where $\tau = U \cdot t/b$

represents the non-dimensional reduced time. The approximation is shown in Figure 3 together with values from the state space formulation of Wagner's function in the SIMPACK User Force Element (UFEL).

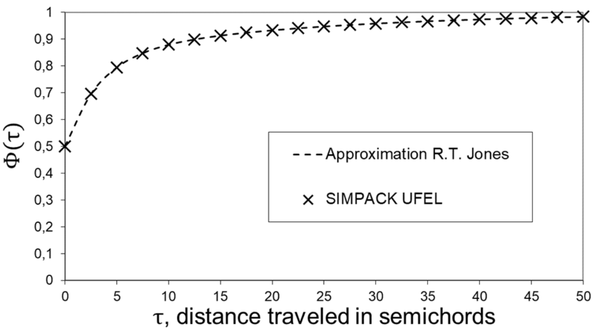

Figure 3: Wagner's function for an incompressible fluid.

As mentioned before, the description of unsteady lift can be extended from an impulsive to a general motion which is illustrated in Figure 4. It includes both, pitch motion α around the elastic axis at $a_h \cdot b$ and heave motion h. In this case one part of the lift arises from circulation, and the other part from non-circulatory apparent mass forces.

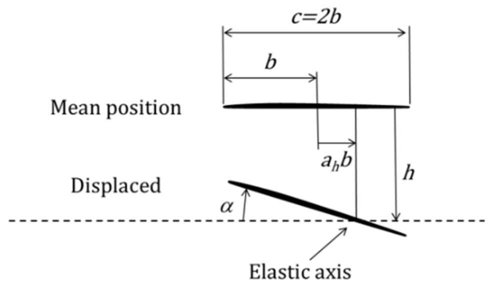

Figure 4: General motion of a two-dimensional airfoil.

To obtain the circulatory lift for the general motion, the measurement of downwash w in heave direction has to be changed from the ¼ chord point to the Pistolesi point at ¾ chord. Here, the quasi-steady downwash of a two-dimensional airfoil undergoing an arbitrary pitch and heave motion around quarter chord (Ref. 10) is given by:

(3) $$w = \alpha U + \dot{\alpha} b + \dot{h}$$

The additional non-circulatory contributions to lift and moment from apparent mass $\rho \cdot \pi \cdot b^2$ and apparent moment of inertia $\rho \cdot \pi \cdot b^2 \cdot (b^2/8)$ must be added for the general motion:

(4) $$L_2 = \rho \pi b^2 \left(\ddot{h} - a_h b \ddot{\alpha}\right)$$

(5) $$L_3 = \rho \pi b^2 U \dot{\alpha}$$

(6) $$M_a = -\frac{\rho \pi b^4}{8} \ddot{\alpha}$$

Hence, total unsteady lift L and moment M about the elastic axis at $a_h \cdot b$, both given per unit span follow as:

(7) $$L = L_1 + L_2 + L_3$$

(8) $$M = \left(\frac{1}{2} + a_h\right) bL_1 + a_h bL_2 - \left(\frac{1}{2} - a_h\right) bL_3 + M_a$$

The lift amplitude and phase obtained for the implemented SIMPACK User Force Element from a harmonic oscillation in angle-of-attack with angular velocity ω are shown in Figure 5 versus the reduced frequency k which is defined as:

(9) $$k = \omega b / U$$

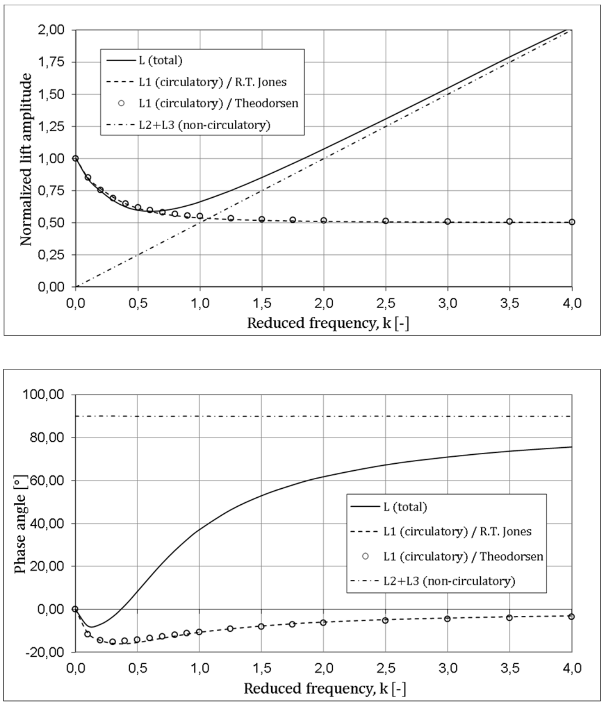

Figure 5: Lift amplitude and phase for circulatory and non-circulatory terms in angle-of-attack oscillation.

The contribution from the circulatory term L_1 is compared to values gained from Theodorsen's function (Ref. 4). In general, the results agree very well for amplitude, but show deviations for phase angle at reduced frequencies around 0.5. Further, the contributions from non-circulatory terms L_2 and L_3 as well as the total lift L closely match the values found in literature (Ref. 3).

2.3. Unsteady Aerodynamics from Axial Inflow and Wake Periodicity

The circulatory part of unsteady lift for the blade airfoil from Wagner function can be extended for rotors under axial flow condition. This requires the consideration of axial dynamic inflow from a non-linear differential equation (Ref. 3) derived out of the results gained by Carpenter and Fridovich (Ref. 6), and wake periodicity as modelled in Loewy's function (Ref. 7) by a complex factor. The associated expressions for axial dynamic inflow and wake periodicity are listed as Eq. (10) and Eq. (11), respectively. They introduce the rotor parameters of rotor angular velocity Ω, inflow λ_i, thrust coefficient C_T, pitch angular velocity ω and blade number N_b.

(10) $$\left(\frac{0.849}{\Omega}\right) \cdot \dot{\lambda}_i + 2 \cdot \lambda_i^2 = C_T$$

(11) $$e^{i \cdot 2\pi \cdot \omega / (N_b \cdot \Omega)} = cos\left(\frac{2\pi \cdot \omega}{N_b \cdot \Omega}\right) + i \cdot sin\left(\frac{2\pi \cdot \omega}{N_b \cdot \Omega}\right)$$

When the blade section starts spinning with angular velocity Ω, an additional downwash due to inflow arises and needs to be considered. In hover with axial inflow, the thrust induced downwash component v_i of a rotor with radius R follows from momentum theory for uniform inflow λ_i as (Ref. 11):

(12) $$\lambda_i = \frac{v_i}{\Omega R} = \sqrt{\frac{C_T}{2}} \quad \text{with} \quad C_T = \frac{T}{\rho \cdot A \cdot \Omega^2 \cdot R^2}$$

(13) $$v_i = \sqrt{\frac{T}{2 \cdot \rho \cdot A}} \quad \text{(global consideration)}$$

(14) $$v_{i,local} = \sqrt{\frac{dT}{2 \cdot \rho \cdot dA}} \quad \text{(local approximation)}$$

The above equations represent a steady inflow condition and result in a constant induced velocity v_i. In accordance with Figure 6, the induced velocity can be either derived under a global consideration for rotor disc area A and thrust T or in terms of a local approach taking the annular segment with area dA and thrust increment dT for the radial station r into account. According thrust coefficients C_T are obtained in the same manner. Thrust and induced velocities are defined normal to the rotor disc.

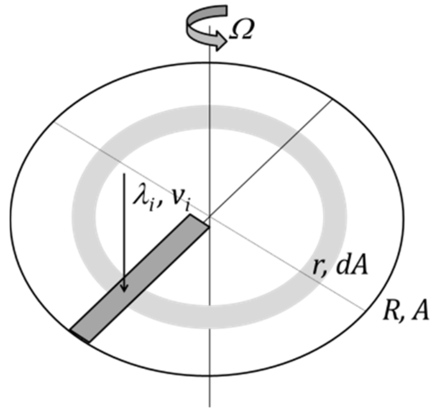

Figure 6: Inflow induced downwash of a rotor blade in axial flight.

Once the steady or dynamic inflow is known with λ_i or $\lambda_i(t)$, the inflow induced velocity v_i is available from Eq. (13) or Eq. (14) and can be considered as a further contribution of downwash. The resulting downwash in hovering flight is found as:

(15) $$w = \alpha U + \dot{\alpha} b + \dot{h} - v_i$$

In the following, dynamic inflow will be modeled with the non-linear first-order ODE from Eq. (10). The solution is a constant inflow for rotor disc area A which depends on thrust coefficient C_T. For the annular segment found at radial station r (see Figure 6) a local thrust coefficient may be derived with segment area dA and inserted in this equation. The obtained inflow value $\lambda_i(t)$ for the rotor disc is then also valid for the local rotor segment. The analytic solution of this equation is found from integral tables for rational functions (Ref. 12) by applying the technique of separated variables, subsequent integration and derivation of the integration constant from the initial inflow condition. This approach leads to the following formulations which need to be solved:

(16) $$\frac{d\lambda_i}{dt} = \left(\frac{C_T \cdot \Omega}{0.849}\right) - \left(\frac{2 \cdot \Omega}{0.849}\right) \cdot \lambda_i^2 = c + a \cdot \lambda_i^2$$

(17) $$\int_{\lambda_i(0)}^{\lambda_i(t)} \frac{d\lambda_i}{c + a \cdot \lambda_i^2} = \int_0^t dt + const.$$

where $a = -\frac{2 \cdot \Omega}{0.849}$ and $c = \frac{C_T \cdot \Omega}{0.849}$

The integration result assumes positive thrust and includes a logarithmic function which is further developed into a kernel expression $\lambda_i(t) = f(C_T, \Phi_\lambda)$ for dynamic inflow that contains the exponential function $\Phi_\lambda(t)$ instead:

(18) $$\lambda_i(t) = \frac{\sqrt{C_T(t) \cdot C_T(0)} \cdot (2 - \Phi_\lambda(t)) + C_T(t) \cdot \Phi_\lambda(t)}{\sqrt{2 \cdot C_T(t)} \cdot (2 - \Phi_\lambda(t)) + \sqrt{2 \cdot C_T(0)} \cdot \Phi_\lambda(t)}$$

The inflow function $\Phi_\lambda(t)$ relates the temporal development for the axial inflow to variations in rotor thrust coefficient C_T and angular velocity Ω in dependence on non-dimensional reduced time τ_λ:

(19) $$\Phi_\lambda(\tau_\lambda) = 1 - e^{-3.3315 \cdot \tau_\lambda} \quad \text{with} \quad \tau_\lambda = \sqrt{C_T} \cdot \Omega \cdot t$$

(20) $$\tau_\lambda = \sqrt{2} \cdot \lambda_i \cdot \Omega \cdot t = \sqrt{2} \cdot \frac{v_i \cdot t}{r}$$

This function is a measure for the inflow change related to a pitch input and introduces a transition effect into the kernel expression $\lambda_i(t)$ with a similar curve shape as depicted in Figure 3 for Wagner's function, but ranging from zero to one. Since the mathematical setup of the axial inflow function resembles Eq. (2), it can be iteratively solved together with the approximated Wagner function to adapt the motion induced lift from Wagner in terms of the thrust input for the inflow induced lift from the axial inflow function. Here, it can be clearly seen from Eq. (19) that no inflow is produced for zero thrust or zero rotation, whilst Eq. (20) highlights that inflow dynamics depends on induced velocity v_i and thus, acts perpendicular to the rotor disc and is detached from reduced time τ used with Wagner function from Eq. (2). This fact allows the evaluation of the inflow induced together with the motion induced unsteady aerodynamic terms in axial flight. Function $\Phi_\lambda(\tau_\lambda)$ (see Figure 7) is related to rotor thrust which can be assumed to be equally distributed over a number of rotor blades in axial flight. Hence, the correlation of dynamic inflow to the blade number N_b is reflected by the model:

(21) $$\tau_\lambda = \sqrt{N_b \cdot C_{T,blade}} \cdot \Omega \cdot t$$

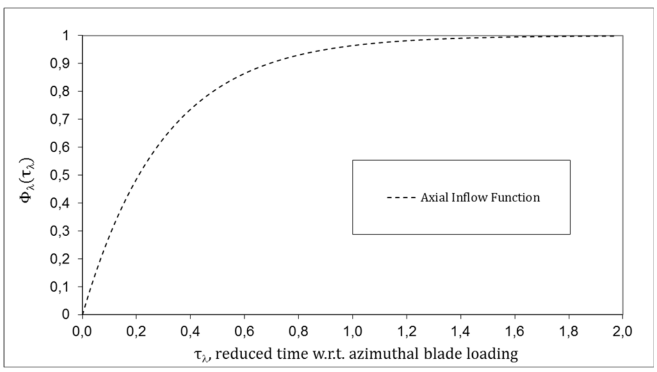

Figure 7: Axial inflow function for an incompressible fluid.

A comparison of the current model comprising Wagner function for motion and axial inflow function for inflow induced unsteady lift with the analytic Loewy function (Ref. 7) from frequency domain reveals the missing contribution of wake periodicity. Equivalent contributions for blade airfoil and axial inflow are found by expressions which are related to reduced frequency k and rotor vortex sheet setup m in the frequency domain model. For completeness, the missing contribution for wake periodicity as modelled in Loewy's function by the complex factor from Eq. (11) is included into the two-dimensional unsteady aerodynamic model for the rotor blade section.

The connection from time to frequency domain and state space is described by the Fourier and Laplace transformation, respectively. Both transformations own the same mathematical mapping rules, but differ in their variables which is imaginary in frequency domain and complex in state space. According to Figure 8, the combination of the periodicity term introducing harmonics w.r.t. the frequency ratio $\omega/(N_b \cdot \Omega)$ with the axial inflow function $\Phi_\lambda(\tau_\lambda)$ is performed in state space by a multiplication leading to an expression $\Phi_\lambda(\tau_\lambda, \omega)$.

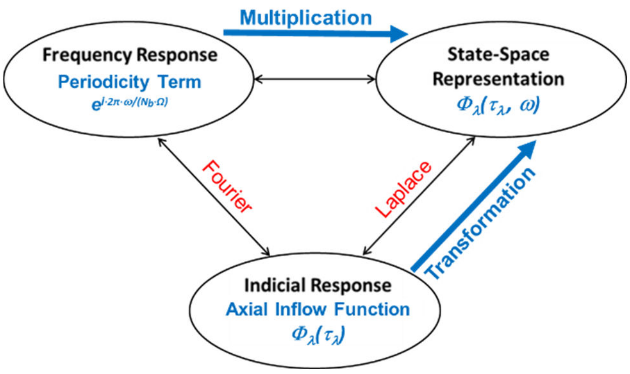

Figure 8: Implementation of wake periodicity term.

2.4. State Space Model

The analytical description for unsteady aerodynamic contributions of the two-dimensional rotor blade section is available in terms of a state space model. As depicted in Figure 9, all contributions of a radial strip can be configured in the model setup of the MBS SIMPACK User Force Element (UFEL).

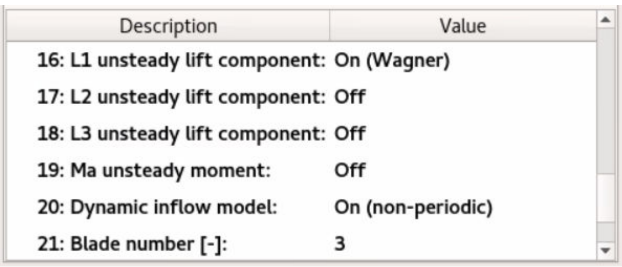

Description	Value
16: L1 unsteady lift component:	On (Wagner)
17: L2 unsteady lift component:	Off
18: L3 unsteady lift component:	Off
19: Ma unsteady moment:	Off
20: Dynamic inflow model:	On (non-periodic)
21: Blade number [-]:	3

Figure 9: Setup of unsteady contributions for rotor blade section in MBS SIMPACK.

The unsteady circulatory contributions of both indicial response functions $\Phi(\tau)$ and $\Phi_\lambda(\tau_\lambda)$ are accounted for by three dynamic states per blade strip. They are implemented in ABCD matrices of the state space system where the values of the rotor contribution are time dependent, since they change with rotor thrust:

$$\left.\begin{aligned} \dot{\mathbf{x}}(t) &= \mathbf{A}\mathbf{x}(t) + \mathbf{B}\mathbf{u}(t) \\ \mathbf{y}(t) &= \mathbf{C}\mathbf{x}(t) + \mathbf{D}\mathbf{u}(t) \end{aligned}\right\} \quad \text{Airfoil contribution (2 states)}$$

$$\left.\begin{aligned} \dot{\mathbf{x}}(t) &= \mathbf{A}(t)\mathbf{x}(t) + \mathbf{B}(t)\mathbf{u}(t) \\ \mathbf{y}(t) &= \mathbf{C}(t)\mathbf{x}(t) \end{aligned}\right\} \quad \text{Rotor contribution (1 state)}$$

The distribution of the circulatory contributions from blade airfoil, rotor inflow and wake periodicity within the matrices of the state space model is sketched in Figure 10 and follows as:

- Wagner Function, approximated (ABCD)
- Carpenter & Fridovich, non-linear ODE (ABC)
- Loewy-function, complex factor (C)

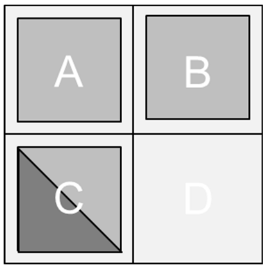

Figure 10: Distribution of circulatory contributions from blade airfoil (light grey), rotor inflow (grey) and wake periodicity (dark grey) in state space matrices.

In the force element, a Newton fix point iteration is applied until the downwash of the airfoil equals axial inflow to obtain the effective angle-of-attack. Finally, the imaginary part of Loewy's periodicity term in Eq. (11) is not used in the model because there is no further imaginary part in the overall equation system.

3. NUMERICAL RESULTS

3.1. Pitch Step in Time Domain

The influence of added rotor inflow on the development of unsteady lift is obtained by applying pitch step excitations in the SIMPACK force element and evaluating the temporal development for the angle-of-attack which is a measure for lift and can be compared to the pitch input. Here, the indicial response for the Wagner function and axial dynamic inflow interacts at each radial station r depending on two separate scales for reduced time, namely τ and τ_λ. The contribution of Wagner's function with τ (rotor in-plane dynamics related to $U = \Omega \cdot r$) reaches the steady state in physical time earlier than the one of axial inflow with τ_λ (rotor out-of-plane dynamics related to $\sqrt{C_T} = \sqrt{2} \cdot \lambda_i$).

As illustrated in Figure 11 for a two-bladed rotor, dynamic axial inflow reduces the effective angle-of-attack for the rotor section, whilst a wing section without inflow follows the basic Wagner function and reaches the commanded pitch angle. Hence, the onset of rotor inflow decreases the angle-of-attack towards a steady value which represents the so-called lift deficiency of a rotor under axial inflow.

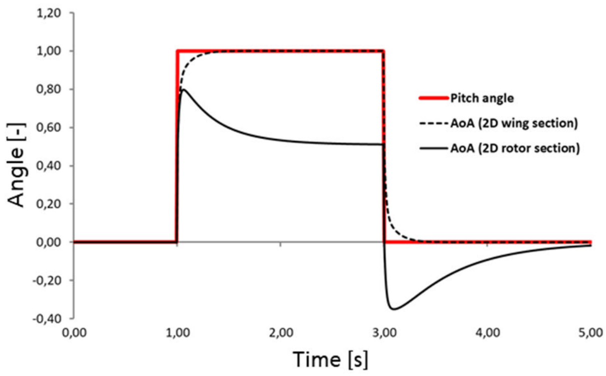

Figure 11: Temporal development of angle-of-attack (AoA) for pitch step input due to axial inflow dynamics.

A comparison for blade number variation with steady values for lift deficiency calculated with the analytical Miller function (Ref. 13) is presented in Table 3 and shows an excellent agreement. The Miller function C holds the following definition:

(22) $$C = \frac{1}{1+(N_b \cdot b/R \cdot \sqrt{2 \cdot C_{T,0}})}$$

Table 3: Lift deficiency from Miller function and SIMPACK UFEL for blade number variation.

Blade Number N_b	Mean Thrust Coefficient $C_{T,0}$	Lift Deficiency (Miller)	Lift Deficiency (Wagner++)
1	0.003255	0.617	0.618
2	0.005248	0.506	0.506
3	0.006967	0.440	0.441
4	0.008263	0.391	0.392

3.2. Pitch Oscillation in Time Domain

To complete the extension of Wagner's function to axial rotor flow, the periodicity term from Loewy's function according to Eq. (11) is implemented in the state space model. The model was carefully tested for harmonic pitch oscillation to gain aerodynamic transfer functions for comparison of the basic Wagner function with the extended models. Figure 12 shows the lift amplitudes and phase angles versus rotor harmonics for the radial section r of a four-bladed rotor (Ω = 62.83 rad/s, $r = 1.0$ m, $b = 0.05$ m, $C_{T,0} = 0.008263$) oscillating around mid chord. The influence of inflow and periodicity related to 4/rev can be seen in both, lift amplitude and phase angle. As predicted by Loewy, reduced damping is found due to a smaller amplitude (Ref. 14-15) and a less negative angle for multiples of the blade passing frequency, i.e. 4/rev and 8/rev. For the used parameters, 1/rev equals a reduced frequency of $k = 0.05$ which is defined as:

(23) $$k = \omega \cdot b/U \quad \text{with} \quad U = \Omega \cdot r$$

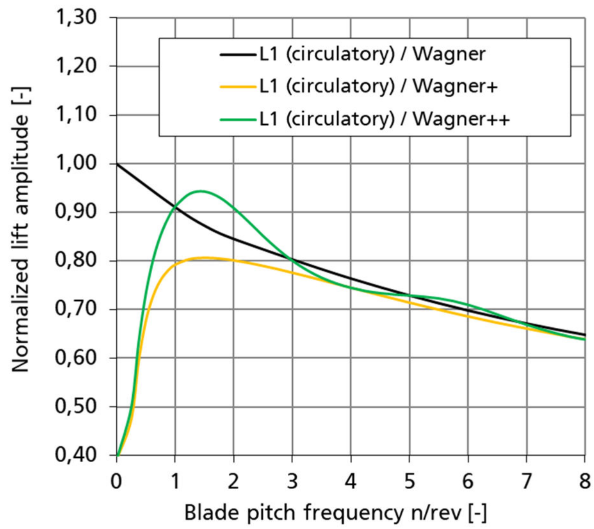

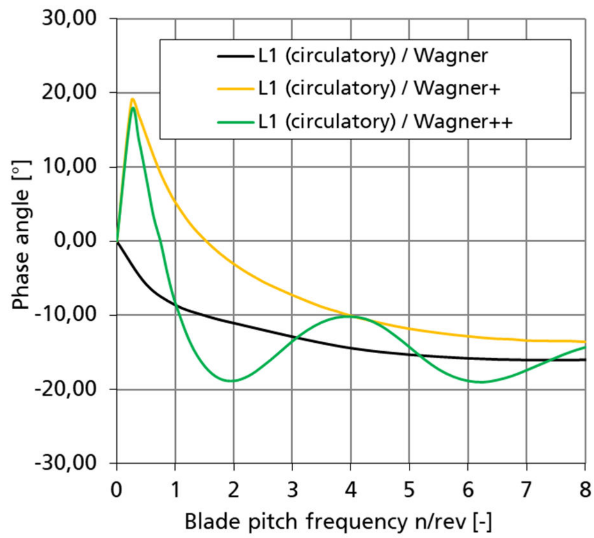

Figure 12: Unsteady lift amplitudes and phase angles of a four-bladed rotor obtained with Wagner function and extensions for rotor inflow (+) and wake periodicity (++).

3.3. Flutter Assessment with Linearization

Standard features in MBS SIMPACK allow the aeroelastic assessment in a tightly-coupled manner on equation level of the rotor blades (Ref. 16-17) for axial inflow condition in time domain and by using linearized results. In the latter approach which is based on linearization, consecutive analysis of the eigenbehaviour and stability rating from damping values can be followed here, since the system matrices for the symmetric rotor with axial inflow remain time invariant and the unsteady aerodynamic forces are considered in the dynamic state set. The analysis is performed with the intrinsic eigensolver and delivers typical flutter results in terms of frequency and damping plots. In general, these results allow the verification of frequency placement and stability for the aeroelastic rotor system.

Since the aerodynamic model is based on indicial response functions, a separation of these contributions is possible and allows for the study of their impact on rotor blade flutter. According flutter results for the straight 7AD (Ref. 16) and double-swept ERATO (Ref. 17) rotor blades were extracted in terms of frequency and damping behaviour for three test cases which differ in the unsteady aerodynamic model for circulation comprising blade airfoil, rotor inflow and wake periodicity.

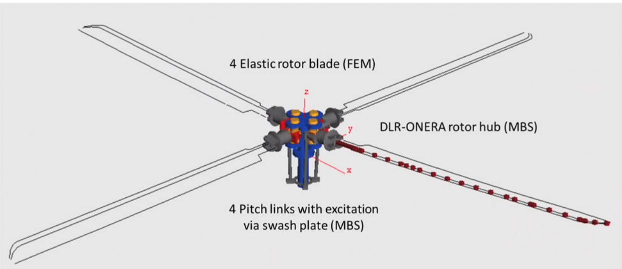

Case	1 / Wagner	2 / Wagner+	3 / Wagner++
Blade airfoil	x	x	x
Rotor inflow		x	x
Wake periodicity			x
Flutter onset	151 %	158 %	158 %

Figure 13: 7AD flutter onset for unsteady aerodynamic models.

As known for articulated rotor blades, also the 7AD blade from Figure 13 exhibits a classical bending-torsion coupling. Here, the lowest flutter onset is found for unsteady aerodynamics limited to blade airfoil, whilst the cases with added rotor inflow and wake periodicity show both the same flutter onset at a 5 % larger rotor speed. In addition to the classical bending-torsion coupling which is well known for articulated straight rotor blades, the double-swept ERATO blade from Figure 14 shows a critical flutter coupling close to nominal rotor speed of 100 % which is composed of two elastic flap bending modes. Due to the forward and backward sweep of the blade layout, these elastic flap modes introduce further torsional blade motion into the aeroelastic coupling and form a blue edge type of flutter coupling that becomes more critical with added rotor inflow and wake periodicity.

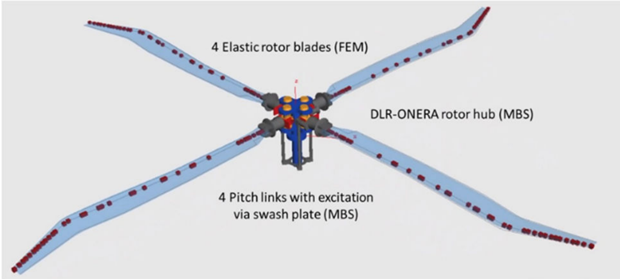

Case	1 / Wagner	2 / Wagner+	3 / Wagner++
Blade airfoil	x	x	x
Rotor inflow		x	x
Wake periodicity			x
Flutter F2-F3 Flutter F5-T1	110 % 128 %	107 % 140 %	107 % 140 %

Figure 14: ERATO flutter onset for unsteady aerodynamic models.

4. CONCLUSIONS AND OUTLOOK

The approach based on indicial aerodynamics ranks as low-fidelity, but offers an efficient and robust method allowing an easy model setup with fast access to basic aeroelastic phenomena at an early design stage. To include methods of different fidelity in the rotor assessment, an aerodynamic multi-fidelity approach around the same dynamic rotor model in MBS SIMPACK is the objective.

The two-dimensional model includes unsteady aerodynamic parts for blade airfoil, axial dynamic inflow and wake periodicity. They are modelled with indicial response functions and implemented in a state space model within the SIMPACK force element. Since the aerodynamic model is state based, numerical solutions are available from time domain and linearization. Related numerical results comprise unsteady aerodynamics for pitch step and oscillation as well as the rotor frequencies and damping for the frequency placement and flutter assessment of isolated rotors.

As part of the future work, the aeroelastic flutter prediction based on indicial aerodynamics and linearization will be included in a multi-disciplinary optimization process for rotor blade design.

Author contact:

Juergen.Arnold@dlr.de

5. REFERENCES

1. https://www.3ds.com/products-services/simulia/products/simpack/
2. Arnold, J., "Flutter Assessment of a Rotor Blade in Steady Axial Flight based on Indicial Aerodynamics," 49th European Rotorcraft Forum, Bückeburg, 2023.
3. Leishman, J. G., *Principles of Helicopter Aerodynamics*, Cambridge University Press, New York, 2nd edition, 2000, Chapter 8.
4. Fung, Y. C., *An Introduction to the Theory of Aeroelasticity*, Dover Publications Inc, New York, 1993, Chapter 6.
5. Wagner, H., "Über die Entstehung des dynamischen Auftriebes von Tragflügeln," *Zeitschrift für angewandte Mathematik und Mechanik*, Band 5, Heft 1, 1925.
6. Carpenter, P. J., and Fridovich, B., "Effect of a Rapid Blade Pitch Increase on the Thrust and Induced Velocity Response of a Full-Scale Helicopter Rotor," NACA TN 3044, 1953.
7. Loewy, R. G., "A Two-Dimensional Approximation to the Unsteady Aerodynamics of Rotary Wings," *Journal of the Aeronautical Sciences*, Vol. 24, No. 2, 1957, pp. 81-92.
8. Arnold, J., and Waitz, S., "Using Multibody Dynamics for the Stability Assessment of a New Rotor Test Rig," 43rd European Rotorcraft Forum, Milan, 2017.
9. Arnold, J., and Waitz, S., "Using Multibody Dynamics for the Stability Assessment of a New Double-Swept Rotor Blade Setup," 44th European Rotorcraft Forum, Delft, 2018.
10. Leishman, J. G. "Modeling of Subsonic Unsteady Aerodynamics for Rotary Wing Applications," AHS Journal, Vol. 35, No. 1, 1990.
11. Padfield, G. D. Helicopter Flight Dynamics: The Theory and Application of Flying Qualities and Simulation Modeling, AIAA Education Series, Blackwell Publishing Ltd, Oxford, 2nd edition, 2007, Chapter 2-3.
12. Bronstein, I. N., and Semendjajew, K. A., Taschenbuch der Mathematik, BSB B. G. Teubner Verlagsgesellschaft, Leipzig, 24th edition, 1989, Chapter 1.1.3.
13. Miller, R. H., "Rotor Blade Harmonic Air Loading, " AIAA Journal, Vol. 2, No. 7, 1964.
14. Ham, N. D., "Helicopter Blade Flutter, " AGARD report No. 607, 1973.
15. Johnson, W., Helicopter Theory, Dover Publications, New York, 1st edition, 1994, Chapter 10.
16. Arnold, J. "Flutter Assessment of a Rotor Blade in Hover Based on Indicial Aerodynamics Considering Blade Profile, Rotor Inflow and Wake Periodicity," 47th European Rotorcraft Forum, Glasgow (virtual), 2021.
17. Arnold, J. "Flutter Assessment of a Double-Swept Rotor Blade in Hover Based on Indicial Aerodynamics Considering Blade Profile, Rotor Inflow and Wake Periodicity," VFS Aeromechanics for Advanced Vertical Flight Technical Meeting, San Jose, 2022.